Separation Science and Technology
Publication details, including instructions for authors and subscription information:
http://www.informaworld.com/smpp/title~content=t713708471

Shell Side Mass Transfer Characteristics in a Parallel Flow Hollow Fiber Membrane Module

Ju-Meng Zheng[a]; You-Yi Xu[a]; Zhi-Kang Xu[a]
[a] Institute of Polymer Science, Zhejiang University, Hangzhou, China

Online publication date: 19 March 2003

To cite this Article Zheng, Ju-Meng , Xu, You-Yi and Xu, Zhi-Kang(2003) 'Shell Side Mass Transfer Characteristics in a Parallel Flow Hollow Fiber Membrane Module', Separation Science and Technology, 38: 6, 1247 — 1267
To link to this Article: DOI: 10.1081/SS-120018808
URL: http://dx.doi.org/10.1081/SS-120018808

MARCEL DEKKER, INC. • 270 MADISON AVENUE • NEW YORK, NY 10016

SEPARATION SCIENCE AND TECHNOLOGY
Vol. 38, No. 6, pp. 1247–1267, 2003

Shell Side Mass Transfer Characteristics in a Parallel Flow Hollow Fiber Membrane Module

Ju-Meng Zheng, You-Yi Xu, and Zhi-Kang Xu*

Institute of Polymer Science, Zhejiang University, Hangzhou, China

ABSTRACT

A cell model was introduced and an analytical solution was obtained to describe the shell side mass transfer problem in a parallel flow hollow fiber membrane module. To develop the analytical model, a uniform fiber arrangement was assumed, and the shell side flow was described by Happel's free surface model, and the boundary condition of a uniform fiber wall concentration was taken into account. The analytical solution showed that the shell side Sherwood number (Sh) was the function of Graetz number (Gz) and the module packing density (Φ). Experiments involving the absorption of CO_2 into water with polypropylene hollow fiber membrane module were performed. It was found that the experimental results could be described by $Sh = (0.163 + 0.27\phi)Gz^{0.6}$. The experimental mass transfer coefficient was higher than that predicted by the model when the packing density of the module was 20%, whereas it was lower than the predicted value when increasing the packing density exceeded 30%. This experimental correlation together with the analytical

*Correspondence: Zhi-Kang Xu, Institute of Polymer Science, Zhejiang University, Hangzhou, China, 310027; E-mail: xuzk@ipsm.zju.edu.cn.

DOI: 10.1081/SS-120018808 0149-6395 (Print); 1520-5754 (Online)

MARCEL DEKKER, INC. • 270 MADISON AVENUE • NEW YORK, NY 10016

solution might provide a useful tool to model and scale up the corresponding membrane contactor process.

Key Words: Hollow fiber membrane module; Membrane contactor; Shell side mass transfer; Analytical solution; CO_2 absorption.

INTRODUCTION

Membrane contactor (MC) processes have got an increasing attention in recent years. Compared with conventional gas/liquid and liquid/liquid contacting devices, MC processes have a great number of advantages including a large and known interface area, the independent control of tube, and shell side flow rate, etc.[1] One of the most commonly used hollow fiber membrane contactor was designed in a tube-shell configuration with shell side fluid parallel to the lumen side fluid, which was either in current or in counter current pattern for each other.

Experimental studies on shell side mass transfer performance in a parallel flow hollow fiber membrane module have been reported widely, as reviewed recently by Lipniski and Field.[2] Most of the approaches described the shell side mass transfer performance on the basis of empirical work.[3–9] However, the results of these studies varied significantly. This might be caused by the irregularity of fiber spacing, the polydispersity of fiber diameters, the fiber movement during operation, the influence of the module wall, and the inlet and outlet effects.

On the other hand, theoretical treatment on shell side mass transfer was based on the assumption of an ordered fiber arrangement. Concerning the counter current hollow fiber dialysis modules, Noda and Gryte[10] found that the effect of entry region was very important. More recently, a numerical solution was obtained by Miyatake and Iwashita for heat transport problem in a parallel flow heat exchanger with different boundary conditions.[11,12] Furthermore, Voronoi tessellation was used to model the fiber distribution and flow distribution in randomly packed fiber bundles with a fluid flowing axially between the hollow fibers.[13,14] The average mass transfer coefficient was estimated from the local mass transfer coefficient in each polygonal cell. Although the mass transfer coefficient in different flow areas could be predicted with Leveque's equation,[6] the mass transfer problem in each cell was not a tube side one in reality.

An analytical solution for the shell side mass transfer with fluid flowing axially between fibers was described in this work. Our primary aim in this study was to explain the discrepancy between the analytical solution and

the observed empirical correlation. Furthermore, the results were compared with the correlation reported in literatures.

THEORY

Model Development

A cell model was developed here to describe the shell side mass transport. To develop the model, the hollow fiber module was divided into small cells with one fiber in each cell, and the free surface appeared in the imaginary outer boundary of the cell.[15] The module was assumed to be uniform packed, and the velocity profile across the module radius direction was ignored. Thus, the shell side mass transfer problem was just the one in the cell. To solve the mass transfer problem in each cell, the following assumptions were used: (1) steady state and isothermal condition; (2) no axial diffusion; (3) using Happel's free surface model[15] to characterize the velocity profile in the cell; (4) the physical properties of the fluid were constant; (5) uniform fiber wall concentration.

Based on these assumptions, the partial differential equation of mass balance and the boundary conditions were as follows:

$$D\left[\frac{\partial^2 \mathrm{c}}{\partial r^2}+\frac{1}{r}\frac{\partial \mathrm{c}}{\partial r}\right]=u\frac{\partial \mathrm{c}}{\partial z} \tag{1}$$

$$r=r_{\mathrm{o}},\quad \mathrm{c}=\mathrm{c}_{\mathrm{i}}$$

$$r=r_{\mathrm{f}},\quad \frac{\partial \mathrm{c}}{\partial r}=0 \tag{2}$$

$$z=0,\quad \mathrm{c}=\mathrm{c}_{\mathrm{in}}$$

Considering surface diffusion on hollow fiber membrane, a uniform fiber surface concentration was assumed as can be seen in Eq. (2). According to Happel's free surface model,[15] the velocity profile in the cell was given by the following equation:

$$u=\frac{2(r_{\mathrm{f}}^2-r_{\mathrm{o}}^2)[r_{\mathrm{o}}^2-r^2+2r_{\mathrm{f}}^2\ln(r/r_{\mathrm{o}})]}{4r_{\mathrm{o}}^2r_{\mathrm{f}}^2-r_{\mathrm{o}}^4-3r_{\mathrm{f}}^4+4r_{\mathrm{f}}^4\ln(r_{\mathrm{f}}/r_{\mathrm{o}})}u_{\mathrm{avg}} \tag{3}$$

where r_o is the fiber out radius and r_f is the free surface radius defined as:

$$r_f = \phi^{-0.5} r_o \tag{4}$$

where Φ is the packing density of the module. And the hydraulic diameter was defined as[15]:

$$d_e = 2(r_f^2 - r_o^2)/r_o = 2\left(\frac{1}{\phi} - 1\right) r_o \tag{5}$$

The differential mass balance in Eq. (1) was made dimensionless by introducing the following dimensionless parameters:

$$f = \frac{r_f}{r_o} \tag{6}$$

$$\eta = \frac{r}{r_o} \tag{7}$$

$$\theta = \frac{c_i - c}{c_i - c_{in}} \tag{8}$$

$$\xi = \frac{(4f^2 - 1 - 3f^4 + 4f^4 \ln f)}{2(f^2 - 1)} \frac{Dz}{r_o^2 u_{avg}}$$

$$= \frac{2(f^2 - 1)(4f^2 - 1 - 3f^4 + 4f^4 \ln f)}{Gz} \tag{9}$$

The partial differential equation and boundary conditions could be written as:

$$\frac{\partial^2 \theta}{\partial \eta^2} + \frac{1}{\eta} \frac{\partial \theta}{\partial \eta} = (1 - \eta^2 + 2f^2 \ln \eta) \frac{\partial \theta}{\partial \xi} \tag{10}$$

$$\eta = 1, \quad \theta = 0$$

$$\eta = f, \quad \frac{\partial \theta}{\partial \eta} = 0 \tag{11}$$

$$\xi = 1, \quad \theta = 1$$

Therefore, the problem became a variant of classis Graetz-Nusselt problem.[16,17] It could be solved with variable separation method.[16,17] Assuming θ was the function of η and ζ, then it could be written in

the following form:

$$\theta = R(\eta)X(\xi) \tag{12}$$

which gave:

$$X' + \lambda^2 X = 0 \tag{13}$$

$$R'' + \frac{1}{\eta}R' + (1 - \eta 2 + 2f^2 \ln \eta)\lambda^2 R = 0 \tag{14}$$

The solution of Eq. (13) was:

$$X = \mathrm{c} \exp(-\lambda^2 \xi) \tag{15}$$

where c is the integral constant. Equation (14) was the Sturm–Liouvill type eigenvalue problem, that could be solved with a Matlab program on a personal computer. Thus, the solution of the partial differential equation would be:

$$\theta = \sum_{n=0}^{\infty} \mathrm{c_n} R_n \exp(-\lambda_n^2 \xi) \tag{16}$$

The constant in Eq. (16) could be calculated as:

$$\mathrm{c_n} = \frac{\int_1^f R_n \eta (1 - \eta^2 + 2f^2 \ln \eta) d\eta}{\int_1^f R_n^2 \eta (1 - \eta^2 + 2f^2 \ln \eta) d\eta} \tag{17}$$

According to film model, the flux of a component was:

$$N_\mathrm{z} = k_\mathrm{z}(\mathrm{c_i} - \mathrm{c_{avg}}) = k_\mathrm{z}\theta_\mathrm{avg}(\mathrm{c_i} - \mathrm{c_{in}}) \tag{18}$$

The average concentration in the shell side should be:

$$\mathrm{c_{avg}} = \frac{2\int_{r_\mathrm{o}}^{r_\mathrm{f}} \mathrm{rucdr}}{(r_f^2 - r_\mathrm{o}^2)u_\mathrm{avg}} \tag{19}$$

Substituting the velocity profile equation into Eq. (19) and integrating, it could be rewritten as:

$$\mathrm{c_{avg}} = \frac{4\int_1^f (1 - \eta^2 + 2f^2 \ln \eta)\eta \mathrm{c} d\eta}{4f^2 - 1 - 3f^4 + 4f^4 \ln f} \tag{20}$$

For there had the following identity:

$$\frac{4\int_1^f (1 - \eta^2 + 2f^2 \ln \eta)\eta d\eta}{4f^2 - 1 - 3f^4 + 4f^4 \ln f} = 1 \tag{21}$$

the expression of the dimensionless concentration was given as:

$$\theta_{avg} = \frac{c_i - c_{avg}}{c_i - c_{in}}$$

$$= \frac{4}{4f^2 - 1 - 3f^4 + 4f^4 \ln f} \sum_{n=0}^{\infty} c_n \exp(-\lambda_n^2 \xi)$$

$$\times \int \eta(1 - \eta^2 + 2f^2 \ln \eta) d\eta \tag{22}$$

Integrating Eq. (14), which gave:

$$\int_1^f \left(\eta \frac{dR}{d\eta}\right) = -\lambda^2 \int_1^f (1 - \eta^2 + 2f^2 \ln \eta) \eta R d\eta \tag{23}$$

Then we got:

$$\lambda_n^2 = \frac{R'n(1)}{\int_1^f (1 - \eta^2 + 2f^2 \ln \eta) \eta R d\eta} \tag{24}$$

Substituting Eq. (24) into Eq. (22), which gave:

$$\theta_{avg} = \frac{4}{4f^2 - 1 - 3f^4 + 4f^4 \ln f} \sum_{n=0}^{\infty} \frac{c_n R'_n(1) \exp(-\lambda_n \xi)}{\lambda_n^2} \tag{25}$$

According to the penetrate model, the flux of a component could also be defined as:

$$N_z = -D\left(\frac{\partial c}{\partial r}\right)_{r=r_o} = \frac{D}{r_o}(c_i - c_{in}) \sum_{n=0}^{\infty} c_n R'_n(1) \exp(-\lambda_n^2 \xi) \tag{26}$$

Combining Eqs. (18), (22), and (26), noting that:

$$Sh_z = \frac{k_z d_e}{D} = \frac{2(f^2 - 1) r_o k_z}{D} \tag{27}$$

the following correlation for the local Sherwood number was obtained:

$$Sh_z = \frac{(f^2 - 1)(4f^2 - 1 - 3f^4 + 4f^4 \ln f)}{2} \frac{\sum_{n=0}^{\infty} c_n R'_n(1) \exp(-\lambda_n^2 \xi)}{\sum_{n=0}^{\infty} c_n R'_n(1) \exp(-\lambda_n^2 \xi)/\lambda_n^2} \tag{28}$$

The expression of the mean Sherwood number could then obtained by using the method suggested by Kays and Crawford[17]:

$$\mathrm{Sh_m} = \frac{(f^2-1)(4f^2-1-3f^4+4f^4\ln f)}{2}\frac{1}{\xi}\ln\frac{1}{\theta_{avg}} \tag{29}$$

Calculation of Experimental Mass Transfer Coefficient

For the absorption of CO_2 into H_2O by hollow fiber membrane contactor, the overall mass transfer resistance was controlled by the liquid phase.[18,19] The average overall mass transfer coefficient K_o could be calculated with following equation[7]:

$$K_o A \Delta C_{lm} = Q_l(C_{out} - C_{in}) \tag{30}$$

where A is the gas–liquid interface area, Q_l is the liquid volumetric flow rate, C_{out} and C_{in} are the outlet and inlet CO_2 concentration in the liquid phase of the module, respectively, and ΔC_{lm} is the log mean driving force given by:

$$\Delta C_{lm} = \frac{(P_{in}/H - C_{in}) - (P_{out}/H - C_{out})}{\ln(P_{in}H - C_{in})/(P_{out}H - C_{out})} \tag{31}$$

in which H is Henry's constant. For CO_2/H_2O system, Henry's constant and diffusivity were found to be[20]:

$$\mathrm{H} = 2.82\times10^{6}\exp(-2044/\mathrm{T}) \tag{32}$$

$$\mathrm{D} = 2.35\times10^{-6}\exp(-2119/\mathrm{T}) \tag{33}$$

The physical–chemical properties such as Henry's constant, diffusivity, density, and viscosity, were assumed to be constant in all experiments.

EXPERIMENTAL

Experiments were conducted to absorb pure CO_2 gas into pure water. The microporous polypropylene hollow fiber membranes (with pore size $0.02\times0.2\,\mu$m, porosity 45%, outer diameter 0.42 mm, and wall thickness 0.04 mm) were supplied by Hualu Ltd, Hangzhou, China. A parallel flow membrane module was used, and it was carefully fabricated by hand. The internal diameter of the module was 10 mm, and the effect fiber length was 200 or 100 mm. The specifications of the module are listed in Table 1. The packing density of the module varied from 20 to 50%, covering the range of practical interesting.

Table 1. Module characteristics and experimental conditions.

No.	Packing density (%)	Fiber number	Effective length (mm)	Hydraulic diameter (mm)	Reynolds number range	Graetz number range
1	20	108	200	1.69	448–1194	1890–5039
2	30	162	200	0.98	215–861	530–2119
3	40	216	200	0.63	179–507	283–503
4	50	270	200	0.42	68–318	70–335
5	20	108	100	1.69	377–1281	3108–10813
6	30	162	100	0.98	246–934	1210–4597
7	40	216	100	0.63	170–528	537–1670
8	50	270	100	0.42	88–528	88–324

A schematic diagram of the experimental apparatus is shown in Fig. 1. Pure water was pumped into the shell side of the module from a feed tank. The inlet pressure of CO_2 was kept at 110 Kpa, and the outlet pressure was kept as atmospheric pressure. CO_2 concentration in the outlet water was measured by titration method.

RESULTS AND DISCUSSION

As mentioned above, the solution of the partial differential equation for mass transfer could be described with Eqs. (28) and (29). It suggested that both

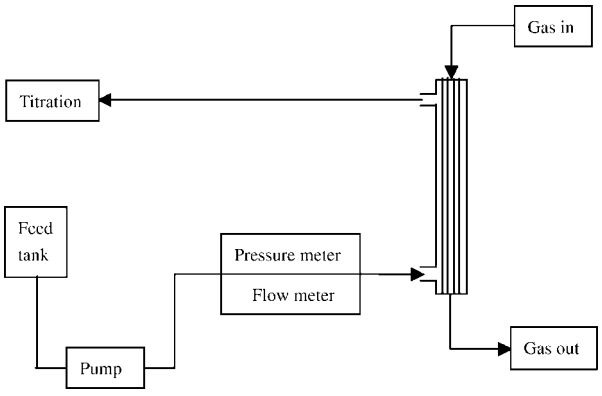

Figure 1. Experimental apparatus for CO_2 absorption.

Table 2. Parameters in Eq. (28) at varies module packing density.

Φ	n	λ^2	$R'(1)$	c
20%	0	0.31876	1.6078	1.1452
	1	4.81145	−4.6366	−0.2101
	2	14.23108	7.2405	0.1150
	≥3		$\lambda_n = 1.5706n + 0.6333$	
			$C_n R'_n(1) = 1.4559\lambda_n^{-1/3}$	
30%	0	1.88445	2.1947	1.1576
	1	26.5193	−6.2428	−0.2148
	2	78.1224	9.7455	0.0870
	≥3		$\lambda_n = 3.6761n + 1.4972$	
			$C_n R'_n(1) = 2.5086\lambda_n^{-1/3}$	
40%	0	8.6237	2.9315	1.1664
	1	115.3824	−8.2383	−0.2330
	2	338.899	12.8537	0.1328
	≥3		$\lambda_n = 7.6676n + 3.0740$	
			$C_n R'_n(1) = 4.5072\lambda_n^{-1/3}$	
50%	0	36.5380	3.9287	1.1747
	1	469.925	−10.9214	−0.2475
	2	1377.01	17.0299	0.1400
	≥3		$\lambda_n = 15.4046n + 6.2989$	
			$C_n R'_n(1) = 7.9524\lambda_n^{-1/3}$	

the local Sherwood number and mean Sherwood number were the function of dimensionless parameter ζ and f, namely, the function of Graetz number and packing density. The parameters in Eq. (28) for different packing density are listed in Table 2. Then, the local Sherwood number could be calculated. The results are shown in Fig. 2. The parameters in Eq. (29) for different packing density are listed in Table 3. The calculated mean Sherwood number versus Graetz number is plotted in Fig. 3.

For practical application, the mean Sherwood number was more useful than the local Sherwood number. From Fig. 3, the mean Sherwood number was correlated with the following correlations when the Graetz number was in the range of 250–2500:

$$\begin{aligned} \mathrm{Sh_m} &= 6.38\mathrm{Gz}^{0.19} \quad (\phi = 20\%) \\ \mathrm{Sh_m} &= 4.67\mathrm{Gz}^{0.22} \quad (\phi = 30\%) \\ \mathrm{Sh_m} &= 3.86\mathrm{Gz}^{0.24} \quad (\phi = 40\%) \\ \mathrm{Sh_m} &= 3.27\mathrm{Gz}^{0.26} \quad (\phi = 50\%) \end{aligned} \tag{34}$$

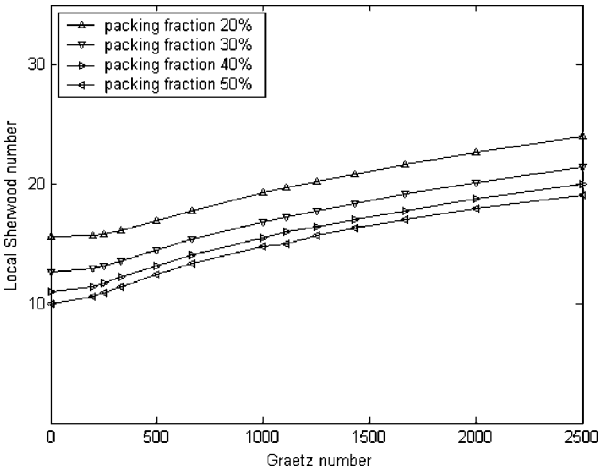

Figure 2. Predicted local Sherwood number vs. logarithm Graetz number at varies packing density.

Table 3. Parameters in Eq. (29) at varies module packing density.

	$\Phi = 20\%$		$\Phi = 30\%$		$\Phi = 40\%$		$\Phi = 50\%$	
Gz	Z	θ_m	ζ	θ_m	ζ	θ_m	ζ	θ_m
∞	0	1	0	1	0	1	0	1
2500	0.0783	0.9477	0.0107	0.9506	0.0020	0.9552	0.0004	0.9559
2000	0.0979	0.9389	0.0134	0.9430	0.0026	0.9466	0.0005	0.9487
1667	0.1175	0.9306	0.0161	0.9358	0.0031	0.9397	0.0007	0.9424
1429	0.1370	0.9228	0.0188	0.9289	0.0036	0.9333	0.0008	0.9362
1250	0.1566	0.9152	0.0215	0.9224	0.0041	0.9273	0.0009	0.9301
1111	0.1762	0.9079	0.0242	0.9160	0.0046	0.9213	0.0010	0.9249
1000	0.1958	0.9009	0.0269	0.9089	0.0051	0.9156	0.0011	0.9189
667	0.2935	0.8683	0.0403	0.8814	0.0077	0.8887	0.0016	0.8952
500	0.3916	0.8386	0.0537	0.8557	0.0102	0.8654	0.0022	0.8709
333	0.5879	0.7849	0.0806	0.8091	0.0153	0.8227	0.0033	0.8298
250	0.7831	0.7365	0.1074	0.7672	0.0204	0.7844	0.0044	0.7939
200	0.9789	0.6915	0.1343	0.7283	0.0256	0.7485	0.0055	0.7609
100	1.9578	0.5059	0.2686	0.5646	0.0511	0.5992	0.0109	0.6222
0	∞	0	∞	0	∞	0	∞	0

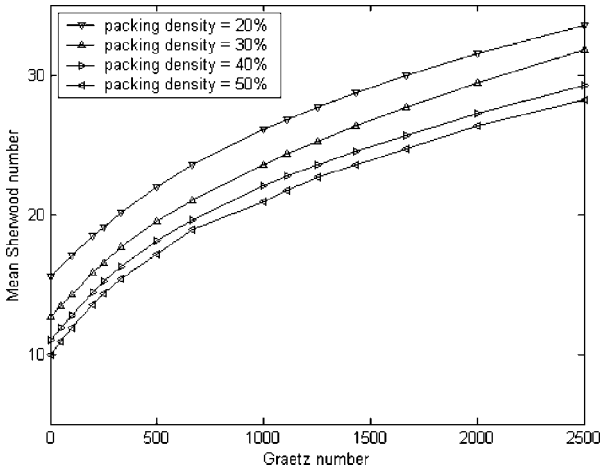

Figure 3. Predicted mean Sherwood number vs. logarithm Graetz number at varies packing density.

For comparison, the mass transport correlations for a triangular arrayed module according to Miyatake and Iwashita's numerical solution[11] were cited as below:

$$\begin{aligned} \mathrm{Sh_m} &= (15.75 + 0.91\mathrm{Gz}^{2/3})^{1/2} \quad (\phi = 20\%) \\ \mathrm{Sh_m} &= (28.55 + 1.61\mathrm{Gz}^{2/3})^{1/2} \quad (\phi = 30\%) \\ \mathrm{Sh_m} &= (45.25 + 2.58\mathrm{Gz}^{2/3})^{1/2} \quad (\phi = 40\%) \\ \mathrm{Sh_m} &= (65.35 + 4.03\mathrm{Gz}^{2/3})^{1/2} \quad (\phi = 50\%) \end{aligned} \tag{35}$$

Both Eqs. (34) and (35) showed that the shell side mass transfer was the function of the Graetz number and the packing density of the module. However, the exponent in the correlations was not a constant, and it was smaller than 1/3 when Eq. (35) was rewritten in the similar form as Eq. (34). It was not surprising to see the discrepancy between the results obtained in this work and those reported by Miyatake and Iwashita.[11] The discrepancy might be due to the different shell flow models, which were adopted to describe the shell side flow. For both situations, the plots of the mean Sherwood number and mass transfer coefficient vs. the packing density are shown in Fig. 4 at a given Graetz number. In Fig. 4a, it can be seen that the value of Sherwood number decreased as the packing

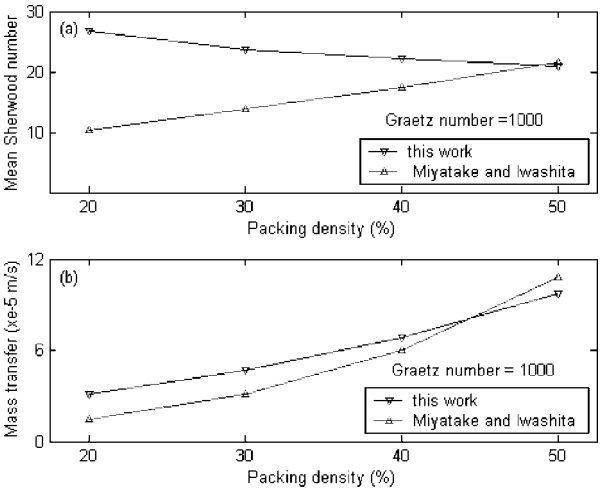

Figure 4. (a) Comparison of the Sherwood number predicted by Miyatake and Iwashita and this work. (b) Comparison of the mass transfer coefficient predicted by Miyatake and Iwashita and this work.

density increased according to our results. But the Miyatake and Iwashita's solution showed an opposite trend. Nevertheless, the plots of the calculated mass transfer coefficient vs. packing density showed a consistent trend in both situations, as shown in Fig. 4b. This might be ascribed to the different definitions of the hydraulic diameter. The hydraulic diameters used by Miyatake and Iwashita and in this work are listed in Table 4, respectively.

The observed mass transfer coefficient was compared with those calculated according to Eqs. (34) and (35). Both experimental and theoretical results are presented in Figs. 5–8 in plot of mass transfer coefficient vs.

Table 4. Value of the hydraulics diameter according to different definition.

Packing density (%)	20	30	40	50
[a]Hydraulic diameter (mm)	1.72	1.01	0.65	0.43
[b]Hydraulic diameter (mm)	1.42	0.88	0.58	0.40

The fiber outer diameter is 0.42 mm, and the module internal diameter is 10 mm.
[a] Definition of hydraulic diameter in this study.
[b] Definition of hydraulic diameter in Miyatake and Iwashita's study.[11]

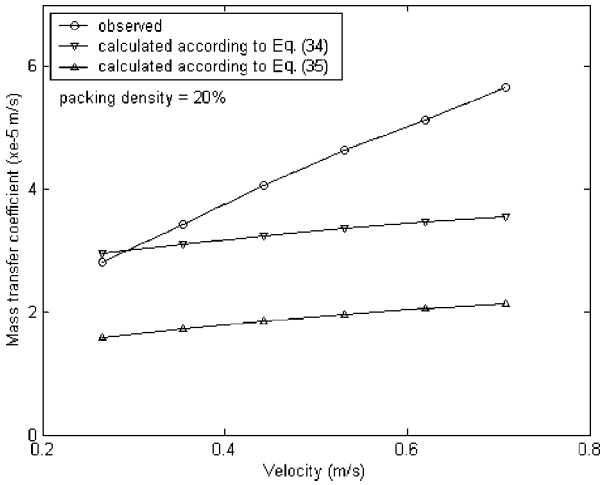

Figure 5. Comparison between the observed and predicted mass transfer coefficient in module 1.

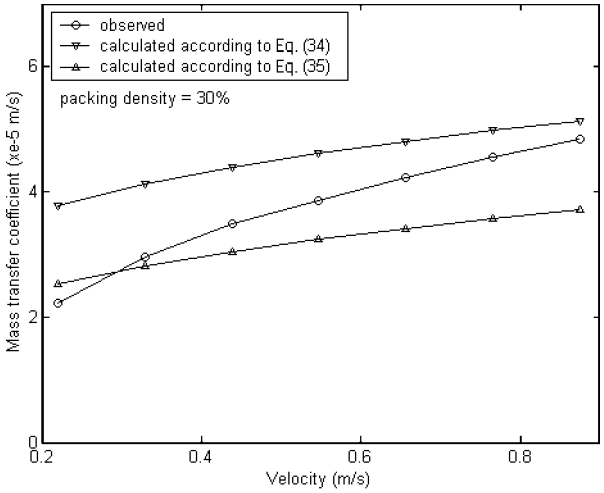

Figure 6. Comparison between the observed and predicted mass transfer coefficient in module 2.

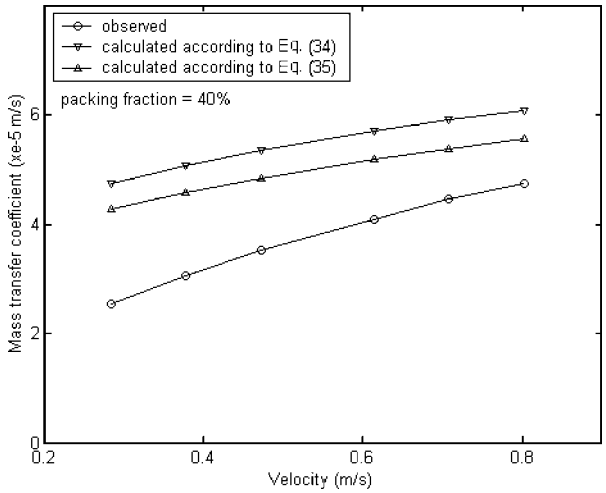

Figure 7. Comparison between the observed and predicted mass transfer coefficient in module 3.

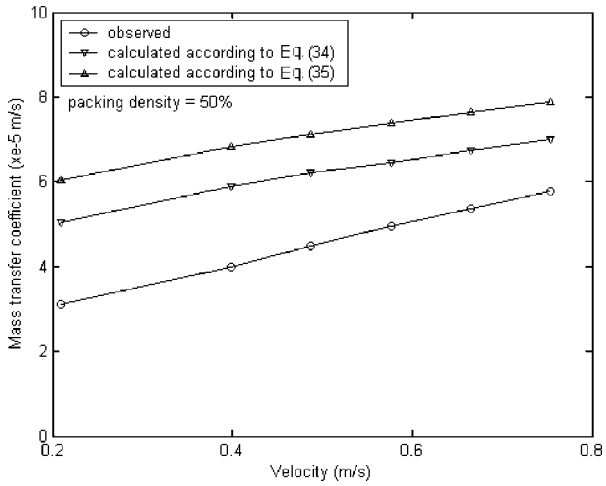

Figure 8. Comparison between the observed and predicted mass transfer coefficient in module 4.

the liquid flow velocity. In these figures, the velocity ranged from 0.2 to 0.8 m/s in each module, whereas the value of Graetz number and Reynolds number varied greatly (as shown in Table 1) due to the quick decrease of the hydraulics diameter with the increase of packing density (see Table 4).

Figure 5 showed that the observed mass transfer coefficient was higher than that calculated by Eqs. (34) or (35) at packing density of 20%. Compared with the model predicted value, enhancement was as high as 70% in this work. And the observed mass transfer coefficient was as much as three times larger than that predicted by Miyatake and Iwashita.[11] These results for loose packed module might be ascribed to the turbulence flow caused by the fiber un-uniform arrangement and large Reynolds number.

In Fig. 6, when the packing density was 30%, it can be found that the observed mass transfer coefficient was not as high as that predicted by our model, but it was larger than the value predicted according to Miyatake and Iwashita's model.[11] For higher packing density, such as 40% and 50%, all the experimental results were lower than the theoretical values, as can be seen from Figs. 7 and 8. The reduction of the mass transfer coefficient might come from the channeling effect and dead zone in the module.

The experimental mass transfer coefficient could be expressed by the following correlation:

$$\mathrm{Sh} = (0.163 + 0.27\phi)\mathrm{Gz}^{0.6} \tag{36}$$

The obvious difference between Eqs. (34) and (35) was that the exponent in Eq. (36) was much larger than that in Eqs. (34) and (35). In model development, the velocity in each cell was the same, and the velocity profile across the whole module was ignored. Considering the velocity profile across the module radial direction, it was reasonable to see large exponent for Graetz number. Data reported in the literature[3–8] also showed the exponent of the Reynolds number about or larger than 0.6 in the mass transfer correlations.

At the same time, the function $f(\Phi)$ decreased in Eq. (34) whereas it increased in Eq. (36) with the increase of packing density. This means that, for a given Graetz number, the Sherwood number decreased with the increase in packing density according to Eqs. (34) or (35), which was contrary to the results of Eq. (36). On the other hand, according to both analytical solution and empirical results, the mass transfer coefficient increased with the increase in packing density, as shown in Fig. 9.

For a particular membrane contactor, the empirical mass transfer coefficient could be predicted by using the correlation:

$$\mathrm{Sh} \propto f(\phi)(d/l)^{\alpha}\mathrm{Re}^{\beta}\mathrm{Sc}^{\gamma} \tag{37}$$

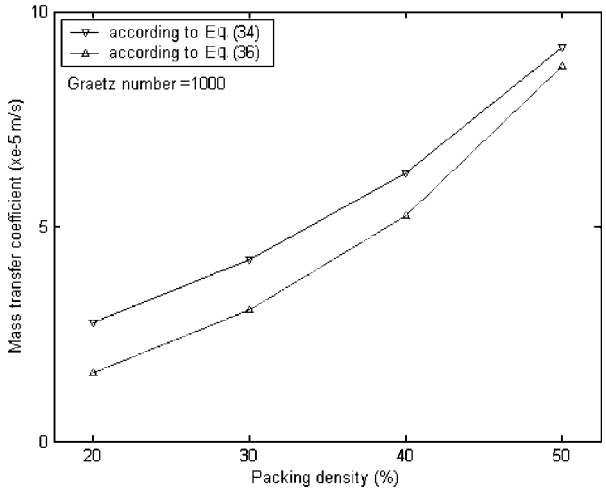

Figure 9. Comparison between analytical solution and empirical correlation at varies packing density for a given value of Graetz number 1000.

The reported correlations in literatures are summarized in Table 5. It can be seen that all these correlations varied greatly in form and were obtained in different experimental conditions. The influence of packing density was not included in the correlations presented by Wickramasinghe et al.,[3] Dahuron et al.,[4] and Yang et al.[5] The correlations of Wu et al.,[6] Costello et al.,[8] and Gawronski et al.[9] showed no dependence of Sherwood number on d_h/L, which implied the stream splitting and recombining repeatedly along the length of the module. It is quite evident that only the empirical correlations proposed by Prasad et al.,[7] Lipnizki et al.,[2] and this work included all parameters presented in Eq. (37). Several correlations were selected to make a comparison in Fig. 10 with the results obtained in this study. To do such comparison, the assumption was made that the empirical correlations can be extrapolated and are not restricted to their experimental conditions. The correlations of Wickramasinghe et al.[3] and Dahuron et al.[4] were excluded because the Sherwood number derived from the former was very close to that of the correlation by Yang et al.,[5] and the value of the latter was much larger than that predicted by other correlations. Furthermore, the correlation of Prasad[7] was not shown in Fig. 10 also due to the much smaller Sherwood number than the other correlations predicted. It can be observed from Fig. 10 that the correlations proposed by Lipnizki et al.,[2] Wickramasinghe et al.,[3]

Table 5. Empirical correlations for shell side mass transfer.

Author	Packing density (%)	Reynolds number range	Correlation
Wickramasinghe	70	$Gz < 60$	$Sh = 0.019Gz$
Dahuron et al.	15		$Sh = 8(Re d_e/l)Sc^{0.33}$
Yang et al.	3, 26	$0 \sim 500$	$Sh = 1.25(Re d_e/l)^{0.93}Sc^{0.33}$
Wu et al.	$8 \sim 70$	$32 \sim 1287$	$Sh = (0.30\phi^2 - 0.34\phi + 0.15)Re^{0.9}Sc^{0.33}$
Prasad et al.	4, 8, 20, 40	$0 \sim 500$	$Sh = 5.8[(1 - \phi)d_e/l]Re^{0.6}Sc^{0.33}$
Costello et al.	$32 \sim 76$	$25 \sim 300$	$Sh = (0.53 - 0.58\phi)Re^{0.53}Sc^{0.33}$
Gawronski et al.	21, 28, 52, 55, 65	$0 \sim 10$	$Sh = 0.09(1 - \phi)Re^{(0.48+0.16\phi)}Sc^{0.33}$
Lipnizki et al.		Laminar	$Sh = ((1.615(1 + 0.14\sqrt[\phi]{4})\sqrt[Re d_e/l]{3})^3 + \left(\left(\frac{2}{22}\right)^{1/6}\sqrt{Re d_e/l}\right)^3)^{1/3}$
This study	20, 30, 40, 50	$178 \sim 1194$	$Sh = (0.163 + 0.27\phi)Gz^{0.60}$

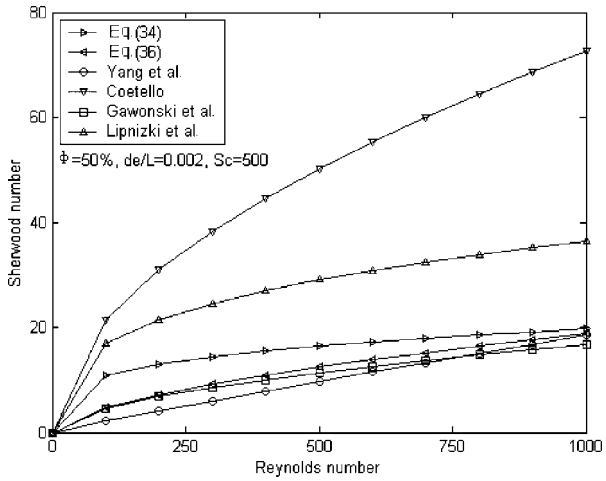

Figure 10. Comparison between the literature correlations and results of this study.

Yang et al.,[5] Wu et al.,[6] and Gawronski et al.[9] showed a relatively close data with our results (including the analytical solution and experimental correlation).

CONCLUSIONS

The shell side mass transfer characteristics of the hollow fiber membrane module were studied both theoretically and experimentally in this article. The analytical solution showed that the Sherwood number was the function of Graetz number and the packing density of the module, and the exponent of the Graetz number in mass transfer correlation was related with packing density. An empirical mass transfer correlation was also given based on the absorption measurements of CO_2 into water. In the case of ignoring the velocity profile across the whole module in model development, the exponent in experimental correlation (0.61) was larger than that in analytical correlation (smaller than 1/3). The ratio of the observed mass transfer coefficient and model predicted value was in the range of 0.7–1.7 in the experimental condition. The analytical solution showed consistency very well with most of the reported correlations, and it might be helpful to model and scale up the membrane contactor process.

LIST OF SYMBOLS

A	interfacial area, m^2
c_i	interfacial concentration, $mol\,m^{-3}$
D	diffusion coefficient, $m^2\,s^{-1}$
d_e	hydraulics diameter, m
f	ratio of fiber outer radius and free surface radius, m
Gz	average Graetz number
H	Herry's coefficient, $Pa\,m^3\,mol^{-1}$
k	mass transfer coefficient, $m\,s^{-1}$
L	fiber length, m
N	flux, $mol\,m^{-2}\,s^{-1}$
P	pressure, Pa
Q_l	volume liquid flow, $m^3\,s^{-1}$
r_o	fiber out radius, m
r_f	free surface radius, m
Re	Reynolds number
Sh	average Sherwood number
T	temperature, K
u	velocity, $m\,s^{-1}$
x	fiber direction
z	axial direction

Greek letters

η	dimensionless defined in Eq. (7)
θ	dimensionless defined in Eq. (8)
λ	dimensionless defined in Eq. (13)
ξ	dimensionless defined in Eq. (9)
ϕ	packing density, %

Subscripts and superscripts

lm	log mean
in	module inlet
out	module outlet
x	local

ACKNOWLEDGMENT

This work was supported by the National Natural Science Foundation of China (Grant No. 59833120).

REFERENCES

1. Gabelman, A.; Hwang, S.-T. Hollow fiber membrane contactors. J. Membr. Sci. **1999**, *159*, 61–106.
2. Lipnizki, F.; Field, R.W. Mass transfer performance for hollow fiber modules with shell-side axial feed flow: using an engineering approach to develop a framework. J. Membr. Sci. **2001**, *193*, 195–208.
3. Wickramasinghe, S.R.; Semmens, M.J.; Cussler, E.L. Mass transfer in various hollow fiber geometries. J. Membr. Sci. **1993**, *69*, 235–250.
4. Dahuron, L.; Cussler, E.L. Protein extraction with hollow fibers. AIChE J. **1998**, *34*, 130–136.
5. Yang, M.-C.; Cussler, E.L. Designing hollow-fiber contactors. AIChE J. **1986**, *32*, 1910–1915.
6. Wu, J.; Chen, V. Shell-side mass transfer performance of randomly packed hollow fiber modules. J. Membr. Sci. **2000**, *172*, 59–74.
7. Prasad, R.; Sirkar, K.K. Dispersion-free solvent extraction with microporous hollow-fiber modules. AIChE J. **1988**, *34*, 177–188.
8. Costello, M.J.; Fane, A.G.; Hogan, P.A.; Schofield, R.W. The effect of shell side hydrodynamics on the performance of axial flow hollow fiber modules. J. Membr. Sci. **1993**, *80*, 1–11.
9. Gawronski, R.; Wrzensinska, B. Kinetics of solvent extraction in hollow-fiber contactors. J. Membr. Sci. **2000**, *168*, 213–222.
10. Noda, I.; Gryte, C.C. Mass transfer in regular arrays of hollow fibers in countercurrent dialysis. AIChE J. **1979**, *25*, 113–121.
11. Miyatake, O.; Iwashita, H. Laminar-flow heat transfer to a fluid flowing axially between cylinders with a uniform surface temperature. Int. J. Heat Mass Transfer **1990**, *33*, 417–425.
12. Miyatake, O.; Iwashita, H. Laminar-flow heat transfer to a fluid flowing axially between cylinders with a uniform wall heat flux. Int. J. Heat Mass Transfer **1991**, *34*, 322–331.
13. Chen, V.; Hlavacek, M. Application of Voronoi tesselation for modeling randomly packed hollow-fiber bundles. AIChE J. **1994**, *40*, 606–612.
14. Rogers, J.D.; Long, R. Modeling hollow fiber membrane contactors using film theory, Voronoi tessellations, and facilitation factors for systems with interface reactions. J. Membr. Sci. **1997**, *134*, 1–17.
15. Happel, J. Viscous flow relative to arrays of cylinders. AIChE J. **1959**, *5*, 174–177.
16. Cussler, E.L. *Diffusion, Mass Transfer in Fluid Systems 2nd*; Cambridge University Press: Cambridge, 1984; 296–302.
17. Kays, W.M.; Crawford, M.E. *Convective Heat and Mass Transfer 2nd*; McGraw-Hill Book Company: New York, 1980; 109–111.

18. Zhang, Q.; Cussler, E.L. Microporous hollow fiber for gas absorption, II. Mass transfer across the membrane. J. Membr. Sci. **1985**, *23*, 333–345.
19. Li, K.; Kong, J.; Tan, X. Design of hollow fiber membrane modules for soluble gas removal. Chem. Eng. Sci. **2000**, *55*, 5579–5591.
20. Kim, Y.-S.; Yang, S.-M. Absorption of carbon dioxide through hollow fiber membrane using various aqueous absorbents. Sep. Purif. Technol. **2000**, *21*, 101–109.

Received February 2002
Revised July 2002